ACS APPLIED MATERIALS & INTERFACES

Letter

www.acsami.org

Green Cobalt Oxide (CoO_x) Film with Nanoribbon Structures Electrodeposited from the BF_2-Annulated Cobaloxime Precursor for Efficient Water Oxidation

Ali Han, Haotian Wu, Zijun Sun, Hongxing Jia, Zhiping Yan, Hao Ma, Xiang Liu, and Pingwu Du*

Department of Materials Science and Engineering, CAS Key Laboratory of Materials for Energy Conversion, University of Science and Technology of China, Hefei, China 230026

Supporting Information

ABSTRACT: In this study, we report for the first time on the use of a water-soluble BF_2-annulated cobaloxime, Co-$(dmgBF_2)_2(OH_2)_2$ (**Co-DMB**, $dmgBF_2$ = difluoroboryl-dimethylglyoxime), as a catalyst precursor for electrocatalytic water oxidation. Oxygen gas bubbles were clearly produced on the FTO electrode at a low overpotential under neutral pH conditions containing **Co-DMB**. Interestingly, stable green films were produced under these conditions. The current densities can reach to >5 mA/cm^2 at 1.1 V and >10 mA/cm^2 at 1.5 V (vs Ag/AgCl). The morphologies of the films showed nanoribbon structures, which were characterized by scanning electron microscope (SEM), energy-dispersive X-ray analysis (EDX), and X-ray photoelectron spectroscopy (XPS).

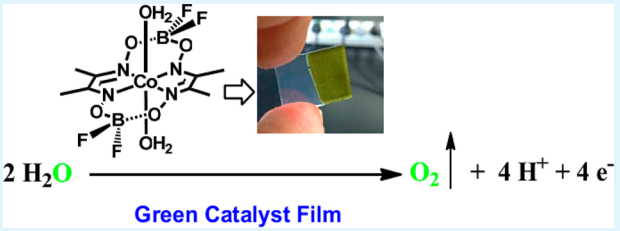

KEYWORDS: *water splitting, cobalt oxide, oxygen production, electrodeposition*

The development of renewable carbon-free energy using the sun is a major scientific and technological challenge in meeting the increasing energy needs of the future.[1,2] Our current energy resources are mainly derived from fossil fuels, which have resulted in numerous environmental problems. Thus, the utilization of solar energy to make carbon-neutral fuels could be an interesting pathway to solve the energy problem and environmental issues. Hydrogen is an ideal energy carrier, but the problem of generating it in an environmentally friendly way and low-cost manner remains to be solved.[3,4] Artificial photosynthesis provides a promising approach to convert solar energy into the form of chemical fuels, for example, producing hydrogen via water splitting.[5−8] Generally, overall water splitting consists of two half reactions: water reduction and water oxidation. Significant progress has been made regarding water reduction in the past decade;[3,4,9,10] however, water oxidation is particularly difficult because it is a $4e^-/4H^+$ process and requires suitable water oxidation catalysts (WOCs) to lower the driving potential ($2H_2O \rightarrow O_2\uparrow + 4H^+ + 4e^-$).[11−13]

Photosynthetic water oxidation can be carried out using a tetranuclear manganese cluster in a membrane-bound protein complex photosystem II (PSII).[14,15] Although metal oxides made of noble metals (mainly Ru[16,17] and Ir[18−20]) show great water oxidation activities, their practical application may be hampered due to their scarcity and high cost.[1,21] Hence, the development of efficient WOCs made of earth-abundant elements, such as metal oxides based on cobalt, nickel, and manganese,[4,10,22,23] is an important subject in the field of solar energy conversion. The WOCs based on cobalt oxide (CoO_x) are of interest for both fundamental and applied research because of their robustness, elemental abundance, and mild operating conditions.[24,25] Many reported cobalt-based WOCs are made starting from inorganic cobalt salts (such as cobalt chloride), which typically show black color with micrometer-sized particles on the electrode.[20,26−28] Previous studies have shown that nanostructured materials might be the key for achieving great catalytic activity for water oxidation.[21,29−32] However, a direct shape control for making novel, nanoscale cobalt-based WOCs using organic precursors has not been well investigated. Thus, we conducted research on organic cobalt complexes as the precursors to discover novel shape-controlled catalysts for water oxidation.

Molecular cobaloximes have received much attention for hydrogen evolution in the past decade (Scheme 1).[9,33,34]

Scheme 1. Molecular Structures of BF_2-Annulated Cobaloximes

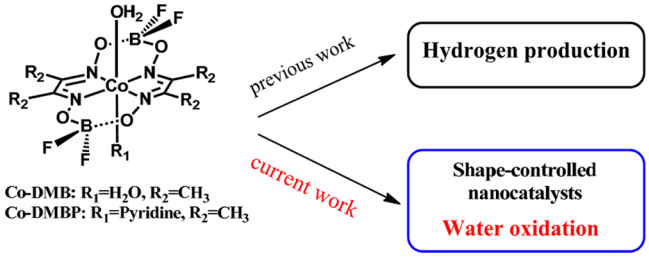

Received: February 8, 2014
Accepted: July 1, 2014
Published: July 1, 2014

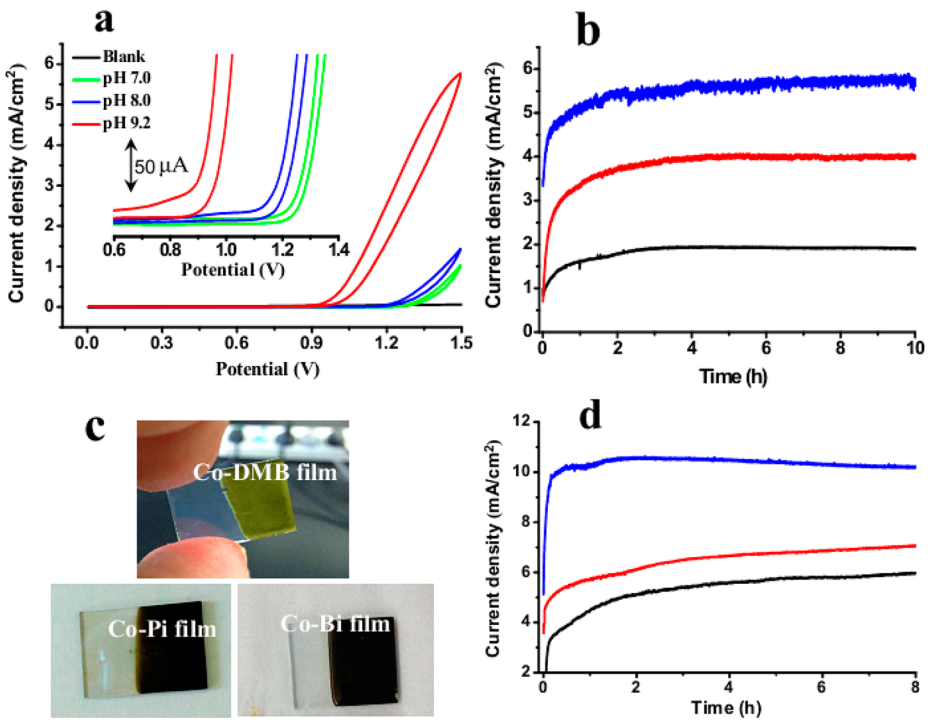

Figure 1. (a) Cyclic voltammograms obtained using FTO working electrodes in 0.1 M buffered solution containing 0.5 mM **Co-DMB**. Red plot, 0.1 M Bi (pH 9.2); blue plot, 0.1 M MePi (pH 8.0); green plot, 0.1 M Pi (pH 7.0). The black plot was recorded as the control test in a 0.1 M Bi (pH 9.2) solution containing no **Co-DMB**. The scan rate was 50 mV/s, and there was *iR* compensation (~5 ohms). (b) Bulk electrolysis of the FTO electrode in 0.1 M Bi solution (pH = 9.2) containing 0.5 mM **Co-DMB** cobaloxime at different potentials. Black, 1.1 V; red, 1.3 V; blue, 1.5 V. (c) The colors of the different Co-based catalysts deposited on the FTO. The upper one represents the **Co-DMB**-based film deposited in Pi buffer at pH 7.0. The lower two display the inorganic Co^{2+}-based Co−Pi film deposited in Pi buffer at pH 7.0 and Co−Bi film deposited in Bi buffer at pH 9.2. (d) Bulk electrolysis of the FTO electrode in a 0.5 M Bi aqueous solution (pH = 9.2) containing 0.5 mM **Co-DMB** at different controlled potentials. Black, 1.1 V; red, 1.3 V; blue, 1.5 V.

However, very few reports have used these for the water oxidation side. Recently, we have reported a series of H-capped cobaloximes as catalyst precursors to deposit uniform cobalt oxide nanoparticles for electrocatalytic water oxidation with good catalytic activity.[26] In the present study, we report novel green cobalt oxide film with nanoribbon structures that is electrodeposited from a BF_2-annulated cobaloxime, Co-$(dmgBF_2)_2(OH_2)_2$ (**Co-DMB**, Scheme 1), as a WOC for oxygen evolution from water. $Co(dmgBF_2)_2(OH_2)Py$ (**Co-DMBP**, Py is pyridine) was used for comparison. The green catalyst film on the fluorine-doped tin oxide (FTO) electrode could efficiently catalyze water oxidation.

Figure 1a shows cyclic voltammetry (CV) scans of FTO as the working electrode in the following media: a 0.5 mM **Co-DMB** in 0.1 M potassium phosphate (Pi) electrolyte at pH 7.0; 0.1 M potassium methylphosphonate (MePi) electrolyte at pH 8.0; and 0.1 M borate (Bi) electrolyte at pH 9.2. Interestingly, a significant catalytic wave is observed with the onset potential of E = 1.17 V in the Pi buffer (note: the potentials in this paper are versus Ag/AgCl). In the MePi electrolyte, the catalytic wave is *n* starting at E = 1.11 V. The corresponding catalytic wave in the Bi electrolyte is much more pronounced with the onset potential of E = 0.89 V. For a fixed catalytic current of 200 μA/cm^2, the observed potentials are 1.34 V for Pi, 1.27 V for MePi, and 0.98 V for Bi electrolyte, respectively. The control experiments show no appreciable catalytic current below 1.5 V in the Bi electrolyte (Figure 1a, black plot), indicating that the presence of **Co-DMB** is essential to the observed catalytic waves.

The apparent catalytic currents for water oxidation prompted us to examine controlled potential electrolysis catalyzed by **Co-DMB**. Water oxidation experiments were carried out at a fixed potential (1.5 V) in 0.1 M Bi electrolyte containing 0.5 mM **Co-DMB**, as shown in Figure 1b (blue plot). At first, the catalytic current rapidly rose, but no film was observed. After 1−2 h, the current density increased to >5.0 mA/cm^2, and a dark green film was apparent on the FTO. The film became thicker as the operating time increased. After 10 h, the stable current density was ~5.8 mA/cm^2. During electrolysis, gas bubbles were clearly observed, and these bubbles have been confirmed as oxygen molecules by gas chromatography and a fluorescence-based oxygen sensor. Moreover, when the applied potentials were 1.3 and 1.1 V, the stable current densities reached ~4.0 and ~1.9 mA/cm^2, respectively. Similar dark green films were also obtained under these conditions. The color of the **Co-DMB** film was different from the Co−Pi and Co−Bi films reported by Nocera and co-workers.[24,25] Generally, the latter two films are black after several hours of electrodeposition (Figure 1c). It should be noted that all of the films were grown under the same conditions. In addition, the **Co-DMB** film is quite stable, and the same current density could be obtained when the fresh prepared film was transferred into a 0.1 M Bi solution containing no **Co-DMB** (Figure S1, Supporting Information). The green films are insoluble in water and in generally available organic solvents in the lab, indicating their heterogeneous character. The absorption spectra of the films formed on FTO plates were measured by UV−vis spectroscopy (Figure S2, Supporting Information). There were obvious broad absorption bands in the visible region, and it is

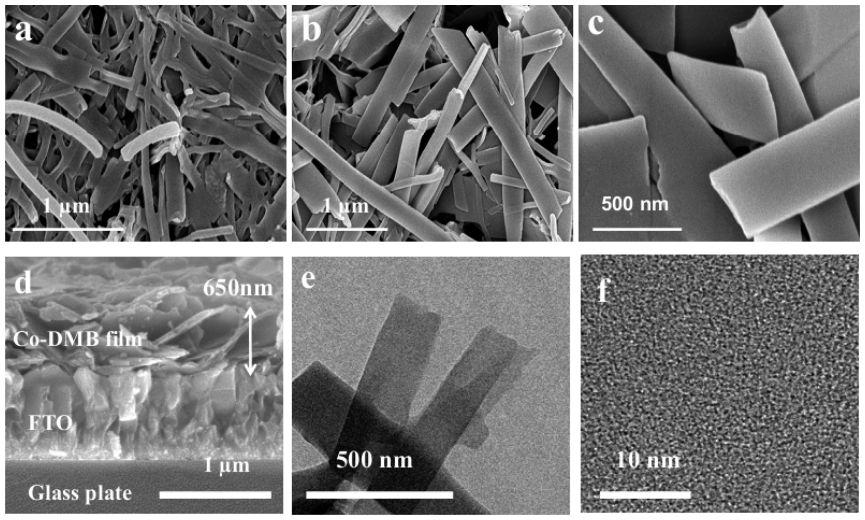

Figure 2. SEM images of **Co-DMB**-based green-colored films deposited on the surface of the FTO at 1.1 V for 10 h in (a) 0.1 M Pi at pH 7.0; (b) 0.1 M MePi at pH 8.0; and (c) 0.1 M Bi at pH 9.2. (d) The cross profile of a green film formed at pH 9.2 in 0.1 M Bi for 10 h. (e) and (f) HR-TEM images of the green film deposited in 0.1 M Bi electrolyte.

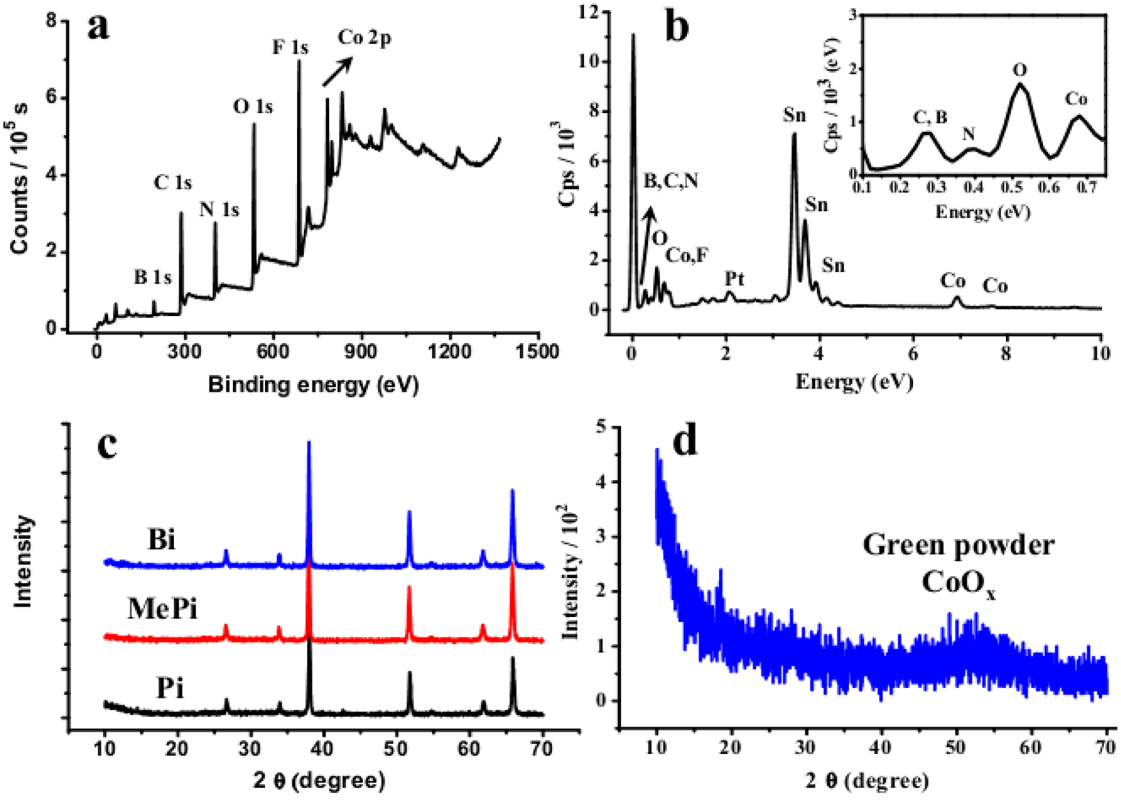

Figure 3. (a) Survey scans of XPS data for a film formed in 0.1 M Bi at pH 9.2; (b) EDX spectrum of the green film formed in 0.1 M Bi at pH 9.2; (c) X-ray diffraction pattern of films formed in three different conditions: black, 0.1 M Pi at pH 7.0; red, 0.1 M MePi at pH 8.0; blue, 0.1 M Bi at pH 9.2; (d) XRD data of the powder scraped from film deposited at pH 9.2 in Bi buffer solution.

difficult to assign the maximum peaks of the green materials in the solid state. In addition, the infrared (IR) spectra of the green colored film and the black Co−Bi film also showed large differences in their functional groups (Figure S3, Supporting Information). For example, the peak of 1634.97 cm^{-1} displays an apparent stretching vibration of −C═N− in the ligand, which is absent in Co−Bi film.

The ionic strength has a significant impact on the catalytic activity. When the Bi electrolyte was used in a fixed concentration of 0.5 M, the values of current densities significantly increased to ~6.0, ~7.0, and ~10 mA/cm^2 under the controlled potentials of 1.1, 1.3, and 1.5 V, respectively (Figure 1d). In contrast to the Co−Pi or Co−Bi catalyst, the formation of green-colored catalyst film also proceeded on the FTO electrode if Bi was replaced by a 0.1 M KCl electrolyte (pH = 9.2, Figure S4a, Supporting Information). However, during bulk electrolysis, the current density rapidly dropped to a level of <0.01 mA/cm^2. When the freshly made green film was

dx.doi.org/10.1021/am500830z | ACS Appl. Mater. Interfaces 2014, 6, 10929−10934

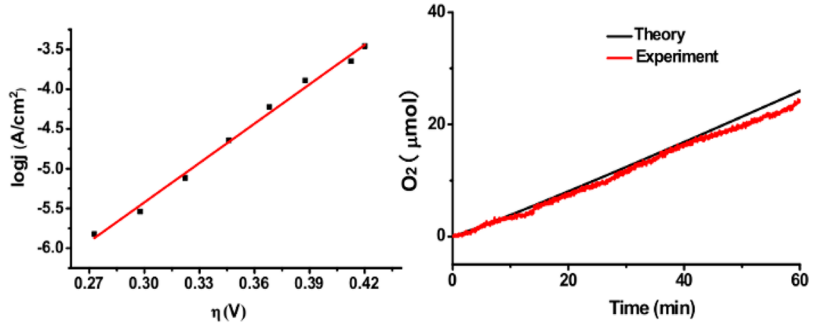

Figure 4. (left) Tafel plot, $\eta = (V_{appl} - iR - E^0)$, of a green film in a 0.1 M Bi buffer at pH 9.2; (right) O_2 detection by a fluorescence-based oxygen sensor. Black plot, theoretical data; red plot, experimental data.

transferred into a 0.1 M Bi electrolyte, the current density increased to ~2.0 mA/cm^2 (Figure S4b, Supporting Information), revealing the crucial roles of the proton-accepting electrolyte for the present catalytic water oxidation. This point of view is also affirmed by the fact that the current density dropped rapidly to <0.4 mA/cm^2 when the green catalyst film deposited in 0.1 M Bi solution was put into a 0.1 M KCl solution (Figure S4c, Supporting Information).

The morphologies of the catalyst films were further characterized by scanning electron microscopy (SEM), as shown in Figure 2 and Figures S5 and S6 (Supporting Information). The images show that all of the deposited materials mainly consist of nanoribbons on FTO, which are novel nanostructures for cobalt oxide-based WOCs deposited from an organic cobalt complex precursor.[26] The widths of the nanoribbons are in the range of 100−400 nm. Some nanoplates are also seen in these SEM images. After 10 h of bulk electrolysis, the thickness of the green film was approximately 650 nm (Figure 2d). The thickness of the present film is in a range similar to previously reported Co-WOCs,[24,25] indicating that the present green color is not due to the **Co-DMB** being thinner than other Co-WOCs. The film grown at pH 9.2 was further examined by high-resolution transmission electron microscopy (HR-TEM), which showed the same nanoribbon structures and an amorphous character (Figure 2e,f). The SEM image of the green film after electrolysis in a 0.1 M Bi solution containing no **Co-DMB** showed similar morphology to the freshly prepared film (Figure S5a, Supporting Information), indicating good morphological stability of the green film before and after the water oxidation reaction. The small particles in Figure S5 (Supporting Information) are the KBi electrolyte. Surprisingly, the film that formed in a 0.1 M KCl solution exhibited very different morphology, lacking nanoribbons and leaving only small particles on the electrode (Figure S5b, Supporting Information). During electrochemical oxidation, the axial ligands of **CoDMB** are possibly cleaved from the cobalt metal center, and the cobalt metal ion strongly interacts with the adjacent complex molecules, resulting in a one-dimensional columnar structure. With the longer time of oxidation, the nanoribbons are formed.

To demonstrate the importance of the ligands to the catalyst film formation, we used a similar cobaloxime, **Co-DMBP**, as the precursor. The CV scans in Figure S7a (Supporting Information) show an apparent catalytic current wave after 1.05 V for the water oxidation reaction. The resulting film exhibited slightly lower current density than **Co-DMB** under the same applied potential. Bulk electrolysis was carried out in a 0.1 M Bi solution at 1.1 V. The stable current density reached ~1.5 mA/cm^2, and a similar green catalyst film was observed (Figure S7b,c, Supporting Information). The SEM image of the green film electrodeposited from **Co-DMBP** also shows nanoribbon structures (Figure S7d, Supporting Information), indicating the ligand containing BF_2 species plays an important role in producing the green film with a controlled morphology. In addition, the CV results also indicate that this catalyst film made of **Co-DMB** precursor exhibits higher catalytic activity than the catalyst film made of Co(dmg)$_2$PyCl precursor (Figure S8, Supporting Information).

The composition and chemical states of the electrodeposited ribbon-like films on the FTO substrate were further analyzed by X-ray photoelectron spectroscopy (XPS), as shown in Figure 3a and Figure S9a−f (Supporting Information). The survey data revealed that all the catalyst films deposited from **Co-DMB** in different electrolytes mainly contained Co 2p, O 1s, C 1s, F 1s, and N 1s, as well as a small peak indicating B 1s. The large F 1s peak could be from both the FTO substrate and the **Co-DMB** precursor. The B 1s may account for the elements in the buffer solution and/or from the cobaloxime precursor. However, unlike the reported Co−Bi catalyst, the peaks of K elements in the present study are not observed, indicating a different composition for the green film.[35] The existence of N, C, F, and B elements suggests the codeposition of dimethylglaoximate ligands, which may control the formation of nanoribbon structures. The characteristic peaks of the Co 2p at 780.91 and 796.21 eV (pH 7.0); 781.47 and 796.27 eV (pH 8.0); and 781.09 and 795.99 eV (pH 9.2) reveal the presence of Co(II) or Co(III) oxide species.[36] The oxygen peak can be attributed to the oxide on the surface of the films.

The green catalyst films were further investigated by energy-dispersive X-ray analysis (EDX) and powder X-ray diffraction (XRD) measurements. The film deposited in Bi buffer mainly contains Co, O, C, and N elements, as well as small amounts of B and F elements (Figure 3b). The Co:C:N ratio is 1.3:2.7:1.0. The C and N elements could be from the cobaloxime precursor. Moreover, both films deposited in buffered solutions at pH 7.0 and pH 8.0 were found to contain a phosphorus element, indicating that both electrolytes were involved in the formation of catalyst films (Figure S10a,b, Supporting Information). The weight ratio of Co:P:C:N is 3.1:1.0:1.5:2.4 for pH 7.0, while the Co:P:C:N ratio is 1.7:0.1:2.7:2.4 for the catalyst deposited in the pH 8.0 buffer. Figure S11 (Supporting Information) shows the EDX data for the catalyst film formed in a 0.1 M KCl solution, which exhibits a different character from the films grown in a Bi-buffered solution. The absence of B, N, and F elements indicated the absence of cobaloxime ligand participation in the formation of the film, suggesting an

important role for the organic ligand in controlling the formation of nanoribbon morphology. The XRD patterns of three electrodeposited catalysts on the FTO show only the peaks associated with the FTO character (Figure 3c). No characteristic peaks are present that indicate the existence of crystalline phases of cobalt oxide, which is consistent with the observations made in the HR-TEM images. Figure 3d shows XRD data of the green-colored catalyst powder scratched from the FTO electrode. An amorphous feature is also observed for the catalyst.

The tafel plot ($\log(j)$ vs η) for the green film deposited in Bi buffer was further studied. The current density for O_2 evolution (j) obtained for the green catalyst film was measured as a function of the overpotential (η). The plot was obtained with a 60 mV/decade, indicating that the catalyst exhibits approximately Nernstian behavior at this pH (Figure 4a). At pH 9.2, appreciable catalytic current is observed beginning at η = 0.25 V. The Faradaic efficiency of the catalyst film was measured using a fluorescence-based oxygen sensor when bulk electrolysis was performed at 1.5 V in 0.1 M Bi buffer at pH 9.2 (Figure 4b). Oxygen detected in the headspace rose with the increase of passed charge. A Faradaic yield of >95% for oxygen production was achieved during electrolysis. Compared with other cobalt-based water oxidation catalysts, the present Co-DMB-based green film shows very good catalytic activity and quite low overpotential for catalytic water oxidation (please see Table S1, Supporting Information). After 1 h of electrolysis, 24.5 μmol of oxygen was detected by the fluorescence sensor. The amount of oxygen increased proportionally with the extension of time.

CONCLUSIONS

In conclusion, this study reports the use of a BF_2-annulated cobaloxime, **Co-DMB**, to deposited cobalt oxide films for electrocatalytic water oxidation. The catalyst films exhibited an interesting green color and nanoribbon structures. Such nanoribbon structures may be controlled by the codeposition of the organic ligands from the cobaloxime precursor. The current density can reach to >5.0 mA/cm^2 at 1.1 V and >10 mA/cm^2 at 1.5 V in a Bi-buffered solution at pH 9.2. A Faradaic yield of >95% was achieved.

ASSOCIATED CONTENT

Supporting Information

Additional characterization data and figures. UV−vis, FT-IR spectra, SEM images, and XPS data. This material is available free of charge via the Internet at http://pubs.acs.org.

AUTHOR INFORMATION

Corresponding Author

*E-mail: dupingwu@ustc.edu.cn.

Notes

The authors declare no competing financial interest.

ACKNOWLEDGMENTS

This work was financially supported by the National Natural Science Foundation of China (21271166), the Fundamental Research Funds for the Central Universities (WK2060140015, WK2060190026), the Program for New Century Excellent Talents in University (NCET), and the Thousand Young Talents Program.

REFERENCES

(1) Gray, H. B. Powering the Planet with Solar Fuel. *Nature* **2009**, *1*, 7.
(2) Lewis, N. S.; Nocera, D. G. Powering the Planet: Chemical Challenges in Solar Energy Utilization. *Proc. Natl. Acad. Sci. U.S.A.* **2006**, *103*, 15729−15735.
(3) Esswein, A. J.; Nocera, D. G. Hydrogen Production by Molecular Photocatalysis. *Chem. Rev.* **2007**, *107*, 4022−4047.
(4) Du, P.; Eisenberg, R. Catalysts Made of Earth-Abundant Elements (Co, Ni, Fe) for Water Splitting: Recent Progress and Future Challenges. *Energy Environ. Sci.* **2012**, *5*, 6012−6021.
(5) Alstrum-Acevedo, J. H.; Brennaman, M. K.; Meyer, T. J. Chemical Approaches to Artificial Photosynthesis. 2. *Inorg. Chem.* **2005**, *44*, 6802−6827.
(6) Meyer, T. J. Chemical Approaches to Artificial Photosynthesis. *Acc. Chem. Res.* **1989**, *22*, 163−170.
(7) Gust, D.; Moore, T. A.; Moore, A. L. Solar Fuels via Artificial Photosynthesis. *Acc. Chem. Res.* **2009**, *42*, 1890−1898.
(8) Hammarström, L.; Hammes-Schiffer, S. Artificial Photosynthesis and Solar Fuels. *Acc. Chem. Res.* **2009**, *42*, 1859−1860.
(9) Dempsey, J. L.; Brunschwig, B. S.; Winkler, J. R.; Gray, H. B. Hydrogen Evolution Catalyzed by Cobaloximes. *Acc. Chem. Res.* **2009**, *42*, 1995−2004.
(10) Artero, V.; Chavarot-Kerlidou, M.; Fontecave, M. Splitting Water with Cobalt. *Angew. Chem., Int. Ed.* **2011**, *50*, 7238−7266.
(11) Tagore, R.; Crabtree, R. H.; Brudvig, G. W. Oxygen Evolution Catalysis by a Dimanganese Complex and Its Relation to Photosynthetic Water Oxidation. *Inorg. Chem.* **2008**, *47*, 1815−1823.
(12) McEvoy, J. P.; Brudvig, G. W. Water-Splitting Chemistry of Photosystem II. *Chem. Rev.* **2006**, *106*, 4455−4483.
(13) Barber, J. Photosynthetic Energy Conversion: Natural and Artificial. *Chem. Soc. Rev.* **2009**, *38*, 185−196.
(14) Ferreira, K. N.; Iverson, T. M.; Maghlaoui, K.; Barber, J.; Iwata, S. Architecture of the Photosynthetic Oxygen-evolving Center. *Science* **2003**, *303*, 1831−1838.
(15) Umena, Y.; Kawakami, K.; Shen, J.-R.; Kamiya, N. Crystal Structure of Oxygen-Evolving Photosystem II at a Resolution of 1.9 Å. *Nature* **2011**, *473*, 55−60.
(16) Harriman, A.; Pickering, I. J.; Thomas, J. M.; Christensen, P. A. Metal Oxides as Heterogeneous Catalysts for Oxygen Evolution under Photochemical Conditions. *J. Chem. Soc., Faraday Trans. I* **1988**, *84*, 2795−2806.
(17) Borgarello, E.; Kiwi, J.; Pelizzetti, E.; Visca, M.; Grätzel, M. Sustained Water Cleavage by Visible Light. *J. Am. Chem. Soc.* **1981**, *103*, 6324−6329.
(18) Zhao, Y.; Hernandez-Pagan, E. A.; Vargas-Barbosa, N. M.; Dysart, J. L.; Mallouk, T. E. A High Yield Synthesis of Ligand-Free Iridium Oxide Nanoparticles with High Electrocatalytic Activity. *J. Phys. Chem. Lett.* **2011**, *2*, 402−406.
(19) Morris, N. D.; Mallouk, T. E. A High-Throughput Optical Screening Method for the Optimization of Colloidal Water Oxidation Catalysts. *J. Am. Chem. Soc.* **2002**, *124*, 11114−11121.
(20) Blakemore, J. D.; Mara, M. W.; Kushner-Lenhoff, M. N.; Schley, N. D.; Konezny, S. J.; Rivalta, I.; Negre, C. F. A.; Snoeberger, R. C.; Kokhan, O.; Huang, J.; Stickrath, A.; Tran, L. A.; Parr, M. L.; Chen, L. X.; Tiede, D. M.; Batista, V. S.; Crabtree, R. H.; Brudvig, G. W. Characterization of an Amorphous Iridium Water-Oxidation Catalyst Electrodeposited from Organometallic Precursors. *Inorg. Chem.* **2013**, *52*, 1860−1871.
(21) Jiao, F.; Frei, H. Nanostructured Cobalt and Manganese Oxide Clusters as Efficient Water Oxidation Catalysts. *Energy Environ. Sci.* **2010**, *3*, 1018−1027.
(22) Dismukes, G. C.; Brimblecombe, R.; Felton, G. A. N.; Pryadun, R. S.; Sheats, J. E.; Spiccia, L.; Swiegers, G. F. Development of Bioinspired Mn_4O_4-Cubane Water Oxidation Catalysts: Lessons from Photosynthesis. *Acc. Chem. Res.* **2009**, *42*, 1935−1943.
(23) Zhou, F.; Izgorodin, A.; Hocking, R. K.; Spiccia, L.; MacFarlane, D. R. Electrodeposited MnO_x Films from Ionic Liquid for Electrocatalytic Water Oxidation. *Adv. Energy Mater.* **2012**, *2*, 1013−1021.

(24) Nocera, D. G. The Artificial Leaf. *Acc. Chem. Res.* **2012**, *45*, 767−776.
(25) Kanan, M. W.; Nocera, D. G. In Situ Formation of an Oxygen-Evolving Catalyst in Neutral Water Containing Phosphate and Co^{2+}. *Science* **2008**, *321*, 1072−1075.
(26) Han, A.; Wu, H.; Sun, Z.; Jia, H.; Du, P. Facile Deposition of Nanostructured Cobalt Oxide Catalysts from Molecular Cobaloximes for Efficient Water Oxidation. *Phys. Chem. Chem. Phys.* **2013**, *15*, 12534−12538.
(27) Singh, A.; Chang, S. L. Y.; Hocking, R. e. K.; Bach, U.; Spiccia, L. Highly Active Nickel Oxide Water Oxidation Catalysts Deposited from Molecular Complexes. *Energy Environ. Sci.* **2013**, *6*, 579−586.
(28) Tian, J.; Li, H.; Asiri, A. M.; Al-Youbi, A. O.; Sun, X. Photoassisted Preparation of Cobalt Phosphate/Graphene Oxide Composites: A Novel Oxygen-Evolving Catalyst with High Efficiency. *Small* **2013**, *9*, 2709−2714.
(29) Wee, T.-L.; Sherman, B. D.; Gust, D.; Moore, A. L.; Moore, T. A.; Liu, Y.; Scaiano, J. C. Photochemical Synthesis of a Water Oxidation Catalyst Based on Cobalt Nanostructures. *J. Am. Chem. Soc.* **2011**, *133*, 16742−16745.
(30) Tüysüz, H.; Hwang, Y. J.; Khan, S. B.; Asiri, A. M.; Yang, P. Mesoporous Co_3O_4 as an Electrocatalyst for Water Oxidation. *Nano Res.* **2013**, *6*, 47−54.
(31) Zhang, F.; Yamakata, A.; Maeda, K.; Moriya, Y.; Takata, T.; Kubota, J.; Teshima, K.; Oishi, S.; Domen, K. Cobalt-Modified Porous Single-Crystalline $LaTiO_2N$ for Highly Efficient Water Oxidation under Visible Light. *J. Am. Chem. Soc.* **2012**, *134*, 8348−8351.
(32) Higashi, M.; Domen, K.; Abe, R. Highly Stable Water Splitting on Oxynitride TaON Photoanode System under Visible Light Irradiation. *J. Am. Chem. Soc.* **2012**, *134*, 6968−6971.
(33) Utschig, L. M.; Silver, S. C.; Mulfort, K. L.; Tiede, D. M. Nature-Driven Photochemistry for Catalytic Solar Hydrogen Production: A Photosystem I-Transition Metal Catalyst Hybrid. *J. Am. Chem. Soc.* **2011**, *133*, 16334−16337.
(34) Du, P.; Knowles, K.; Eisenberg, R. A Homogeneous System for the Photogeneration of Hydrogen from Water Based on a Platinum(II) Terpyridyl Acetylide Chromophore and a Molecular Cobalt Catalyst. *J. Am. Chem. Soc.* **2008**, *130*, 12576−12577.
(35) Surendranath, Y.; Dinca, M.; Nocera, D. G. Electrolyte-Dependent Electrosynthesis and Activity of Cobalt-Based Water Oxidation Catalysts. *J. Am. Chem. Soc.* **2008**, *131*, 2615−2620.
(36) Bomben, K. D.; Moulder, J. F.; Sobol, P. E.; Stickel, W. F. *Handbook of X-Ray Photoelectron Spectra: A Reference Book of Standard Spectra for Identification*; Perkin Elmer: Eden Prairie, MN, 1992.